https://doi.org/10.5194/egusphere-2025-861
Preprint. Discussion started: 26 June 2025

Chloric Acid-Driven Nucleation Enhanced by Dimethylamine and Sulfuric acid in the Arctic: Mechanistic Study

Shengming Wang[1], Huidi Zhang[2], Xiangli Shi[2], Qingzhu Zhang[1,*], Wenxing Wang[1], Qiao Wang[1]

[1]Environment Research Institute, Shandong University, Qingdao 266237, P. R. China

[2]College of Geography and Environment, Shandong Normal University, Jinan 250014, PR China

Keywords: New particle formation, Chloric acid, Particle formation rate, Cluster concentration, Atmospheric nucleation precursor

*Corresponding authors. E-mail:zqz@sdu.edu.cn.

https://doi.org/10.5194/egusphere-2025-861
Preprint. Discussion started: 26 June 2025

Abstract

Chlorine radicals are strong oxidizing agents in the atmosphere, and the process of chlorine oxidation results in the formation of chloric acid ($HClO_3$, CA). Recent studies have shown that CA is prevalent in the Arctic boundary layer. However, the contribution of chlorine-containing species to oceanic new particle formation (NPF) has not been fully revealed. It is expected that CA is involved in the oceanic nucleation process. In this study, the enhancement of CA-based NPF by dimethylamine (DMA) and sulfuric acid (SA) was comparatively investigated at the molecular level using density-functional theory (DFT) and atmospheric cluster dynamics simulation (ACDC). The results show that DMA can form clusters with CA through hydrogen bonding, halogen bonding and proton transfer, which reduces the energy barrier for CA-based cluster formation and significantly improves the thermodynamic stability of CA clusters. The cluster formation rate of CA-DMA cluster system is higher than that of the CA-SA cluster system. The CA-DMA cluster system in the Arctic atmosphere contributes to NPF. These findings may help to reveal some of the missing sources of the Arctic NPF. The present study contributes to a deeper understanding of the influence of oceanic chlorine-containing constituents on the oceanic NPF.

https://doi.org/10.5194/egusphere-2025-861
Preprint. Discussion started: 26 June 2025

1 Introduction

Marine aerosols as the main natural aerosol system have a major global impact by regulating the radiative balance and climate of clouds(O' dowdg). New particle formation (NPF) contributes to more than half of the global cloud condensation nuclei, which in turn contributes to cloud formation (Gordon et al., 2017; Takegawa et al., 2020; Williamson et al., 2019; Zhang et al., 2012). Compared with clouds over land, ocean clouds cover a wider area and significantly increase the albedo of the ocean, so ocean clouds contribute more to the climate system (Merikanto et al., 2009; Wood, 2012; Zheng et al., 2021). Sulfuric acid (SA, H_2SO_4), methane sulfonic acid (MSA, CH_3HSO_3), and iodic acid (IA, HIO_3) are generally considered to contribute to the formation of oceanic particles (Hodshire et al., 2019; Yin et al., 2021; Facchini et al., 2008; Perraud et al., 2015; Arquero et al., 2017; Hopkins et al., 2008). However, there is still a significant difference between the particle formation rates observed in the field and those predicted by simulation (Kirkby et al., 2011; Kirkby et al., 2016; Zhang et al., 2004; Ehn et al., 2014; Dawson et al., 2012). Therefore, it is necessary to consider whether other gaseous precursors are involved in NPF to narrow the gap between experiments and simulations.

Compared to the main atmospheric oxidants, hydroxyl radicals, chlorine radicals act as strong oxidants in the polar troposphere at relatively high concentration levels (Stone et al., 2012). The active chlorine cycle in the Arctic boundary layer during the spring after polar sunrise depletes O_3 in the region (Custard et al., 2016; Foster et al.,

https://doi.org/10.5194/egusphere-2025-861
Preprint. Discussion started: 26 June 2025

2001; Thompson et al., 2015). Chloric acid (CA) has no photoactivity and CA is ubiquitous in the spring in the Arctic, with concentrations estimated to range from 1×10^5 to 7×10^6 molecules cm^{-3} (Tham et al., 2023). CA was not found in the particle phase of the aerosol, thus it is difficult to determine whether CA is involved in the NPF phase.

Many studies have shown that atmospheric bases such as methylamine (MA), dimethylamine (DMA), trimethylamine (TMA) and ammonia can effectively enhance SA-based NPF (Yao et al., 2018; Almeida et al., 2013). Although amines emit 10−20 times less than ammonia in the ocean, amines can effectively form clusters with substances such as SA in the ocean (Myriokefalitakis et al., 2010; Semeniuk and Dastoor, 2018; Almeida et al., 2013). Of these amines, DMA has been found as a component of marine secondary aerosols (Facchini et al., 2008). Widely dispersed DMA has an atmospheric concentration of 0.4 − 10 pptv over the ocean and plays a key role in marine NPF(Van Pinxteren et al., 2019). DMA has been identified as the strongest enhancing atmospheric amine for SA and IA-driven NPF (Olenius et al., 2017; Ning et al., 2022). Thus, DMA may have a higher enhancing potential (EP) than NH_3 for CA-based NPF.

Sulfuric acid (H_2SO_4, SA) has been detected in both gas and particulate phases in polluted coastal areas of China(Zhu et al., 2019; Yu et al., 2019). It is noteworthy that the concentration of SA is two orders of magnitude higher (up to 10^8 molecules cm^{-3}) in the coastal polluted areas due to urban air pollution compared to the clean marine atmosphere(Zhu et al., 2019). Considering its strong nucleation ability(Sipilä et al.,

https://doi.org/10.5194/egusphere-2025-861
Preprint. Discussion started: 26 June 2025

2010; Faloona, 2009), it is likely that SA molecules nucleate in marine regions along with CA.

Using density functional theory (DFT) and the Atmospheric Clusters Dynamic Code (ACDC), the involvement of DMA and SA in the initial phase of CA-based NPF has been investigated. We obtained the minimum free energy structures of the $(CA)_{1-4}(DMA)_{1-4}$ and $(CA)_{1-4}(SA)_{1-4}$ clusters. The temperatures used in this study are within the temperature range of the atmospheric boundary layer in the ordinary range(Mířijovský and Langhammer, 2015). The concentration of CA was estimated to be in the range of $1.0 \times 10^6 - 1.0 \times 10^8$ molecules cm^{-3} based on measured data. Further study of CA-DMA clusters under Arctic atmospheric conditions and the corresponding thermodynamic data used as input to the ACDC reveals the growth pathways and formation rates of the clusters.

2 Computational methods

Configurational Sampling

We employed a multi-step global minimum sampling scheme to search for the global minimum of $(CA)_{1-4}(DMA)_{1-4}$ and $(CA)_{1-4}(SA)_{1-4}$ clusters. In this study, the initial structures of 1000-10000 $(CA)_{1-4}(DMA)_{1-4}$ and $(CA)_{1-4}(SA)_{1-4}$ clusters were randomly generated using the ABCluster software to determine their global minima (clusters with the lowest Gibbs free energies). In the multistep sampling scheme, the geometry optimization is performed at the PM7, ωB97X-D/6-31+G(d,p) and ωB97X-D/6-31++G(d,p) levels of theory, and the single-point energy calculations are

https://doi.org/10.5194/egusphere-2025-861
Preprint. Discussion started: 26 June 2025

performed at the DLPNO-CCSD(T)/aug-cc-pVTZ level of theory based on the ωB97X-D/6-31++G(d,p) theory level is performed on the geometry. The GAUSSIAN 09 program package(Frisch et al., 2016) was used to perform the PM7 and ωB97X-D calculations. DLPNO-CCSD(T) calculations were performed in the ORCA 4.0.0 program(Neese, 2012). For convergence problems and failures such as ending with a false frequency in the optimization of $(CA)_{1-4}(DMA)_{1-4}$ and $(CA)_{1-4}(SA)_{1-4}$ cluster geometries, the initial structures will be modified and re-optimized until the optimization is successful. The free energy of formation (ΔG) of individual clusters is calculated at different temperatures 238, 258, and 278 K. The ΔG of individual clusters is calculated at different temperatures. The structures of $(SA)_{1-4}$ and $(DMA)_{1-4}$ clusters were obtained from previous studies and are recalculated here(Xie et al., 2017).

Atmospheric Cluster Dynamics Code (ACDC) Simulation

Time-evolving cluster formation rates, steady-state concentrations, and growth paths for $(CA)_{1-4}(DMA)_{1-4}$ and $(CA)_{1-4}(SA)_{1-4}$ clusters were calculated using ACDC(Mcgrath et al., 2012). There is good agreement between the conclusions of the ACDC simulations and the experimental results obtained using the birth and death equations (Almeida et al., 2013; Lu et al., 2020; Kürten et al., 2018). In this study, ACDC simulations were performed to model the formation process of CA-DMA and CA-SA neutral clusters without considering the effects of charge and water. The $(CA)_5(DMA)_5$ clusters are set as boundary clusters (see Supporting Information (SI) for details). The concentration ranges of [CA], [SA] and [DMA] were set to 10^6-10^8

https://doi.org/10.5194/egusphere-2025-861
Preprint. Discussion started: 26 June 2025

cm^{-3}, 10^6-10^8 cm^{-3} and 0.1−100 ppt, respectively.

3 Results and discussion

3.1 Cluster Structures and Cluster Formation Free Energy

To evaluate the thermodynamic stability of the formed CA-DMA clusters, the formation free energies (ΔG, kcal mol^{-1}) at 278 K are calculated for the $(CA)_{1-4}(DMA)_{1-4}$ clusters at the DLPNO-CCSD(T)/aug-cc-pVTZ//ωB97X-D/6-31++G(d,p) level of theory. As shown in Figure. 1, hydrogen bonds play an important role in the formation of CA-DMA clusters. Proton transfer reactions are not observed in the pure $(CA)_2$ and $(CA)_3$ clusters, whereas spontaneous proton transfer reactions are observed in all $(CA)_{1-4}(DMA)_{1-4}$ clusters. For most $(CA)_{1-4}(DMA)_{1-4}$ clusters, protons are transferred from CA to DMA.

In order to compare the thermodynamic stability of the formed CA-DMA and CA-SA clusters, we calculated the formation Gibbs free energy values (ΔG, kcal mol^{-1}) for the $(CA)_{1-4}(DMA)_{1-4}$ clusters at 278 K at the DLPNO-CCSD(T)/aug-cc-pVTZ//ωB97X-D/6-31++G(d,p) level of theory. As shown in Figure. 1, hydrogen bonding plays an important role in the formation of CA-DMA clusters. Proton transferring wasn't observed in pure $(CA)_2$ and $(CA)_3$ clusters, whereas spontaneous proton transfer reactions were present in all $(CA)_{1-4}(DMA)_{1-4}$ clusters. For most $(CA)_{1-4}(DMA)_{1-4}$ clusters, protons are transferred from CA to DMA, forming Cl-O...H-N hydrogen bonding, accompanied by the production of

https://doi.org/10.5194/egusphere-2025-861
Preprint. Discussion started: 26 June 2025

ClO_3^- negative ions and DMA^+ ions. In CA-DMA clusters containing two or more chlorine atoms, including $(CA)_2(DMA)_1$, $(CA)_3(DMA)_1$, $(CA)_3(DMA)_1$, $(CA)_3(DMA)_1$, $(CA)_3(DMA)_4$, $(CA)_4(DMA)_1$, $(CA)_4(DMA)_2$, $(CA)_4(DMA)_3$, and $(CA)_4(DMA)_4$ clusters, O-O...O-Cl halogen bonds and Cl-O...H-N hydrogen bonds together stabilize these clusters described above. Halogen bonds are not present in clusters containing single CA atom and in $(CA)_2(DMA)_2$, $(CA)_2(DMA)_3$, $(CA)_2(DMA)_4$, as well as $(CA)_3(DMA)_3$ clusters. For the CA-SA clusters, the ClO_3^- negative ions generated in the CA-DMA cluster system were not found in the CA-SA cluster system because proton transfer do not occur. In contrast to the O-Cl...O-Cl halogen bond found in the CA-DMA cluster system, the CA-SA cluster adds S-O...Cl-O halogen bond (in the Figure S2).

The formation Gibbs free energy values of (A) $(CA)_{1-4}(DMA)_{1-4}$ and (B) $(CA)_{1-4}(SA)_{1-4}$ at 278 K and 1 atm are shown in Figure. 2. The Gibbs free energy values for the formation of $(CA)_2$, $(CA)_3$, and $(CA)_4$ clusters in the pure acid system are 1.31, 2.52, and 5.37 kcal mol^{-1}, respectively, implying that at 278 K, pure CA clusters are thermodynamically difficult to form. The ΔG values of $(CA)_1(SA)_4$ and pure SA clusters are lower than the corresponding ΔG values of the corresponding CA-DMA system. The difference between the ΔG values of $(CA)_4(DMA)_4$ cluster and $(CA)_4(SA)_4$ cluster is the largest, up to 61.62 kcal mol^{-1}. $(CA)_1(SA)_1$ and $(CA)_1(DMA)_1$ are both very important in their respective cluster systems, and their ΔG values are −2.62 and 10.08 kcal mol^{-1}, respectively^{-1}. The ΔG values of $(CA)_{1-4}$ clusters are 10.08 − 28.16 kcal mol^{-1} higher than those of the corresponding

https://doi.org/10.5194/egusphere-2025-861
Preprint. Discussion started: 26 June 2025

$(CA)_{1-4}(DMA)_1$ clusters, suggesting that pure CA clusters may grow by collision with DMA. As the size of CA-DMA clusters increases, the clusters gradually form a cage-symmetric structure. The ΔG values of the majority of clusters in the CA-DMA system are 3.55 − 61.62 kcal mol^{-1} lower than the corresponding ΔG values of the CA-SA system. This indicates that the CA-DMA cluster system is more thermally stable compared to the CA-SA cluster system.

3.1 Evaporation Rates and Cluster Stability

The total evaporation rate ($\sum\gamma$, s^{-1}) of $(CA)_{1-4}(DMA)_{1-4}$ clusters and $(CA)_{1-4}(SA)_{1-4}$ clusters formed at T = 278 K is shown in Figure. 3. The smaller value of $\sum\gamma$ means that the stability of CA-DMA clusters is higher and the clusters shrink further. The smaller value of $\sum\gamma$ implies the higher stability of CA-DMA clusters and further contraction of the clusters. The clusters with the same number of CA molecules and the number of DMA molecules include $(CA)_1(DMA)_1$, $(CA)_2(DMA)_2$, $(CA)_3(DMA)_3$, and $(CA)_4(DMA)_4$ clusters, which have the values of $\sum\gamma$ of 10^2, 2×10^{-4}, 5×10^{-1}, and 3×10^1 s^{-1}, respectively. $(CA)_2(DMA)_2$ cluster has the lowest $\sum\gamma$ value, implying that $(CA)_2(DMA)_2$ cluster is the most stable cluster in the "4 × 4" box system of CA-DMA clusters. For clusters with different numbers of CA and DMA molecules, the $\sum\gamma$ value of $(CA)_2(DMA)_1$ cluster is significantly lower than that of other clusters, which indicates that $(CA)_2(DMA)_1$ cluster has a high probability of competing for the growth path of nucleation. In this study, we compare the evaporation rates of clusters from the CA-DMA system with those from the CA-SA

https://doi.org/10.5194/egusphere-2025-861
Preprint. Discussion started: 26 June 2025

system at 278K. In contrast to the other clusters, the evaporation rate of $(CA)_1(SA)_4$ clusters is lower than that of the corresponding $(CA)_1(DMA)_4$ clusters. The evaporation rates of most $(CA)_{1-4}(DMA)_{1-4}$ clusters are much smaller than those of the corresponding $(CA)_{1-4}(SA)_{1-4}$ clusters, indicating that the CA-DMA cluster system is kinetically more stable than the CA-SA cluster system.

3.2 Cluster Formation Rates and Steady-State Cluster Concentrations

Cluster formation rate (J) and steady-state CA dimer concentration ($\sum[(CA)_2]$) are important indicators for assessing the enhancement potential of DMA for CA-based nucleation. Figure 4 shows the variation of $\sum[(CA)_2]$ and J values at 278 K with CA concentration ([CA] = $10^6 - 10^8$ cm^{-3}) and DMA concentration ([DMA] = 1, 10 and 100 ppt). The J value of the CA-DMA system showed a positive correlation with CA and DMA concentrations as CA and DMA concentrations increased. The dependence of the cluster formation rate on the DMA concentration does not decrease with increasing CA concentration, which means that the dependence of the system on DMA does not saturate when the CA concentration is high. The $\sum[(CA)_2]$ and J of the CA-DMA system with the full range of acid-base concentrations considered (CA: $10^6 - 10^8$ molecules cm^{-3}, DMA: 1, 10 and 100 ppt) were significantly higher than the CA-SA system (Figure. S4). However, at high concentrations of [CA] = 1×10^7 molecules cm^{-3} and [DMA] = 10 ppt, the J value of the CA-DMA cluster system only reaches 6.70×10^{-7} cm^{-3} s^{-1}. The contribution of the CA-DMA cluster system to the NPF is not significant under the atmospheric conditions of 278 K. In addition, the

https://doi.org/10.5194/egusphere-2025-861
Preprint. Discussion started: 26 June 2025

CA-PA cluster system has a lower *J* value (Figure. S15). This may be due to the weak bond energies of Cl-O...Cl-O halogen bonds in the process of CA-PA nucleation.

To further systematically explore the effect of temperature on the *J* of the CA-DMA cluster system, Figure. 5 shows the simulated *J* at other temperatures (238 and 258 K), [CA] = 10^6 − 10^8 molecules cm^{-3}, [DMA] = 0.1 ppt (red line), 1 ppt (green line), 10 ppt (blue line), and 100 ppt (black line). A comparison of the simulations at 258 K (Figure. 5a) and 238 K (Figure. 5b) reveals that the decrease in temperature further increases the *J* value of the CA-DMA cluster system to a higher level. However, at a low temperature (258 K), the *J* values of the CA-DMA cluster system do not reach higher levels at high concentrations of [CA] = 1 × 10^7 molecules cm^{-3} and [DMA] = 10 ppt. The *J* values of the CA-DMA cluster system were further investigated under cold Arctic conditions (238 K). It was found that the *J* value of CA-DMA cluster system at 238 K atmospheric condition was significantly higher than that of CA-DMA cluster system at other higher temperature conditions, which was mainly due to the fact that the low temperature attenuates the evaporation of CA-DMA clusters.

3.3 Cluster growth pathway

Figure 6 shows the growth paths of CA-DMA and CA-SA clusters at 278 K, [CA] = 10^6 cm^{-3}, [DMA] = 1 ppt, and [SA] = 10^6 cm^{-3}. The first step in the growth of CA-DMA clusters is the collision of a CA molecule and a DMA molecule to form a $(CA)_1(DMA)_1$ cluster. There are two growth paths for $(CA)_1(DMA)_1$ clusters: a CA

https://doi.org/10.5194/egusphere-2025-861
Preprint. Discussion started: 26 June 2025

molecule collides and combines with a $(CA)_1(DMA)_1$ cluster to form a $(CA)_2(DMA)_1$ cluster, and a DMA molecule is subsequently added to form a $(CA)_2(DMA)_2$ cluster; a $(CA)_1(DMA)_1$ cluster combines with another $(CA)_1(DMA)_1$ cluster to form a $(CA)_2(DMA)_2$ cluster. This growth pattern is mainly due to the high stability of $(CA)_2(DMA)_1$ clusters. After the $(CA)_2(DMA)_2$ clusters, the growth route of the CA-DMA cluster system extends along the direct binding to the $(CA)_1(DMA)_1$ clusters. For $(CA)_3(DMA)_3$ clusters, one route is the addition of acid and base, and the other route is the direct binding to $(CA)_1(DMA)_1$ clusters to produce $(CA)_4(DMA)_4$ clusters.

The growth pathway of the CA-SA cluster system differs considerably from that of the CA-DMA cluster system. The cluster initially formed in the CA-SA cluster system is the $(CA)_2$ cluster not the $(CA)_1(SA/DMA)_1$ cluster in the CA-DMA system. After the generation of $(CA)_2$ cluster, the system can generate $(CA)_3(SA)_1$ clusters by successive addition of acid molecules. Subsequently, $(CA)_3(SA)_1$ clusters combine with $(CA)_1(SA)_1$ clusters to generate $(CA)_3(SA)_2$ clusters. The final $(CA)_4(SA)_4$ cluster of the system is generated by collision of a $(CA)_3(SA)_2$ cluster with an $(SA)_2$ cluster.

3.4 Atmospheric implications and conclusions

In this paper, combination method of quantum chemistry and ACDC were used to elucidate the molecular structure mechanism of DMA and SA enhancing role of CA nucleation by comparing the CA-DMA and CA-SA nucleation systems. Proton

https://doi.org/10.5194/egusphere-2025-861
Preprint. Discussion started: 26 June 2025

transfer was observed in all $(CA)_{1-4}(DMA)_{1-4}$ clusters while no proton transfer occurred within $(CA)_{1-4}(SA)_{1-4}$ clusters. The ClO_3^- groups generated by the deprotonation of CA are involved in the formation of at least one hydrogen bond. Hydrogen and halogen bonds together stabilize the CA-DMA and CA-SA nucleation systems. The vast majority of CA-SA cluster systems have higher ΔG values than the corresponding CA-DMA cluster systems. The cluster formation rates of the pure CA-PA and CA-SA nucleation systems are relatively low, and the contribution of DMA to CA nucleation is stronger than that of SA. The CA-DMA nucleation system contributes to the NPF at low Arctic temperatures. Clusters with the same number of CA and DMA molecules ($(CA)_1(DMA)_1$, $(CA)_2(DMA)_2$, $(CA)_3(DMA)_3$, and $(CA)_4(DMA)_4$ clusters) play a key role in the growth path of CA-DMA clusters. This study is important for a deeper understanding of CA Arctic atmospheric nucleation.

The study clarifies the role of CA in the marine NPF and reveals the mechanism of DMA acting as a key enhancer to CA-based NPF through intermolecular interactions. The results suggest that CA-DMA synergistic nucleation in the Arctic atmosphere is an under-recognized source of NPF, which provides a theoretical basis for improving regional climate models (e.g., cloud condensation nucleation prediction) and assessing the Arctic aerosol-climate feedback effect. The current simulations do not take into account charge effects, the involvement of water molecules, and the influence of complex atmospheric matrices (e.g., organic matter). In the future, it is necessary to validate the simulation results with field observations and extend it to multi-component (e.g., IA/SA/DMA mixing) nucleation systems in order to quantify

https://doi.org/10.5194/egusphere-2025-861
Preprint. Discussion started: 26 June 2025

the contribution of chlorine-containing substances to the global NPF in a more comprehensive way.

Data availability

All data supported the paper are available from the article, supplementary information，and the corresponding author upon reasonable request.

Acknowledgements

The work was financially supported by National Natural Science Foundation of China (project No. 22236004, 21976107, 42175122, 4217050207) and Taishan Scholars (No. ts201712003).

Additional information

Competing interests: The authors declare no competing financial interests.

https://doi.org/10.5194/egusphere-2025-861
Preprint. Discussion started: 26 June 2025

References

Almeida, J., Schobesberger, S., Kürten, A., Ortega, I. K., Kupiainen-Määttä, O., Praplan, A. P., Adamov, A., Amorim, A., Bianchi, F., and Breitenlechner, M.: Molecular understanding of sulphuric acid–amine particle nucleation in the atmosphere, Nature, 502, 359-363, 2013.

Arquero, K. D., Xu, J., Gerber, R. B., and Finlayson-Pitts, B. J.: Particle formation and growth from oxalic acid, methanesulfonic acid, trimethylamine and water: a combined experimental and theoretical study, Physical Chemistry Chemical Physics, 19, 28286-28301, 2017.

Custard, K. D., Pratt, K. A., Wang, S., and Shepson, P. B.: Constraints on Arctic atmospheric chlorine production through measurements and simulations of Cl2 and ClO, Environ. Sci. Technol., 50, 12394-12400, 2016.

Dawson, M. L., Varner, M. E., Perraud, V., Ezell, M. J., Gerber, R. B., and Finlayson-Pitts, B. J.: Simplified mechanism for new particle formation from methanesulfonic acid, amines, and water via experiments and ab initio calculations, Proceedings of the National Academy of Sciences, 109, 18719-18724, 2012.

Ehn, M., Thornton, J. A., Kleist, E., Sipilä, M., Junninen, H., Pullinen, I., Springer, M., Rubach, F., Tillmann, R., and Lee, B.: A large source of low-volatility secondary organic aerosol, Nature, 506, 476-479, 2014.

Facchini, M. C., Decesari, S., Rinaldi, M., Carbone, C., Finessi, E., Mircea, M., Fuzzi, S., Moretti, F., Tagliavini, E., and Ceburnis, D.: Important source of marine secondary organic aerosol from biogenic amines, Environmental science & technology, 42, 9116-9121, 2008.

Faloona, I.: Sulfur processing in the marine atmospheric boundary layer: A review and critical assessment of modeling uncertainties, Atmospheric Environment, 43, 2841-2854, 2009.

Foster, K. L., Plastridge, R. A., Bottenheim, J. W., Shepson, P. B., Finlayson-Pitts, B. J., and Spicer, C. W.: The role of Br2 and BrCl in surface ozone destruction at polar sunrise, Science, 291, 471-474, 2001.

Frisch, M., Trucks, G., Schlegel, H., Scuseria, G., Robb, M., Cheeseman, J., Scalmani, G., Barone, V., Petersson, G., and Nakatsuji, H.: Gaussian 16, Revision A. 03, Gaussian, Inc., Wallingford CT, 3, 2016.

Gordon, H., Kirkby, J., Baltensperger, U., Bianchi, F., Breitenlechner, M., Curtius, J., Dias, A., Dommen, J., Donahue, N. M., and Dunne, E. M.: Causes and importance of new particle formation in the present-day and preindustrial atmospheres, Journal of Geophysical Research: Atmospheres, 122, 8739-8760, 2017.

Hodshire, A. L., Campuzano-Jost, P., Kodros, J. K., Croft, B., Nault, B. A., Schroder, J. C., Jimenez, J. L., and Pierce, J. R.: The potential role of methanesulfonic acid (MSA) in aerosol formation and growth and the associated radiative forcings, Atmospheric Chemistry and Physics, 19, 3137-3160, 2019.

Hopkins, R. J., Desyaterik, Y., Tivanski, A. V., Zaveri, R. A., Berkowitz, C. M., Tyliszczak, T., Gilles, M. K., and Laskin, A.: Chemical speciation of sulfur in marine cloud droplets and particles: Analysis of individual particles from the marine boundary layer over the California current, Journal of Geophysical Research: Atmospheres, 113, 2008.

Kirkby, J., Curtius, J., Almeida, J., Dunne, E., Duplissy, J., Ehrhart, S., Franchin, A., Gagné, S., Ickes, L.,

https://doi.org/10.5194/egusphere-2025-861
Preprint. Discussion started: 26 June 2025

and Kürten, A.: Role of sulphuric acid, ammonia and galactic cosmic rays in atmospheric aerosol nucleation, Nature, 476, 429-433, 2011.

Kirkby, J., Duplissy, J., Sengupta, K., Frege, C., Gordon, H., Williamson, C., Heinritzi, M., Simon, M., Yan, C., and Almeida, J.: Ion-induced nucleation of pure biogenic particles, Nature, 533, 521-526, 2016.

Kürten, A., Li, C., Bianchi, F., Curtius, J., Dias, A., Donahue, N. M., Duplissy, J., Flagan, R. C., Hakala, J., and Jokinen, T.: New particle formation in the sulfuric acid–dimethylamine–water system: reevaluation of CLOUD chamber measurements and comparison to an aerosol nucleation and growth model, Atmospheric Chemistry and Physics, 18, 845-863, 2018.

Lu, Y., Liu, L., Ning, A., Yang, G., Liu, Y., Kurtén, T., Vehkamäki, H., Zhang, X., and Wang, L.: Atmospheric sulfuric acid - dimethylamine nucleation enhanced by trifluoroacetic acid, Geophysical Research Letters, 47, e2019GL085627, 2020.

McGrath, M., Olenius, T., Ortega, I., Loukonen, V., Paasonen, P., Kurtén, T., Kulmala, M., and Vehkamäki, H.: Atmospheric Cluster Dynamics Code: a flexible method for solution of the birth-death equations, Atmospheric Chemistry and Physics, 12, 2345-2355, 2012.

Merikanto, J., Spracklen, D., Mann, G., Pickering, S., and Carslaw, K.: Impact of nucleation on global CCN, Atmospheric Chemistry and Physics, 9, 8601-8616, 2009.

Miřijovský, J. and Langhammer, J.: Multitemporal monitoring of the morphodynamics of a mid-mountain stream using UAS photogrammetry, Remote sensing, 7, 8586-8609, 2015.

Myriokefalitakis, S., Vignati, E., Tsigaridis, K., Papadimas, C., Sciare, J., Mihalopoulos, N., Facchini, M., Rinaldi, M., Dentener, F., and Ceburnis, D.: Global modeling of the oceanic source of organic aerosols, Adv, Meteorol, 939171, 2010.

Neese, F.: The ORCA program system, Wiley Interdisciplinary Reviews: Computational Molecular Science, 2, 73-78, 2012.

Ning, A., Liu, L., Zhang, S., Yu, F., Du, L., Ge, M., and Zhang, X.: The critical role of dimethylamine in the rapid formation of iodic acid particles in marine areas, npj Climate and Atmospheric Science, 5, 92, 2022.

O ' DowdG, C.: de Leeuw, " , Marine aerosol production: a review of the current knowledge, 1753-1774,

Olenius, T., Halonen, R., Kurtén, T., Henschel, H., Kupiainen-Määttä, O., Ortega, I. K., Jen, C. N., Vehkamäki, H., and Riipinen, I.: New particle formation from sulfuric acid and amines: Comparison of monomethylamine, dimethylamine, and trimethylamine, Journal of Geophysical Research: Atmospheres, 122, 7103-7118, 2017.

Perraud, V., Horne, J. R., Martinez, A. S., Kalinowski, J., Meinardi, S., Dawson, M. L., Wingen, L. M., Dabdub, D., Blake, D. R., and Gerber, R. B.: The future of airborne sulfur-containing particles in the absence of fossil fuel sulfur dioxide emissions, Proceedings of the National Academy of Sciences, 112, 13514-13519, 2015.

Semeniuk, K. and Dastoor, A.: Current state of aerosol nucleation parameterizations for air-quality and climate modeling, Atmos. Environ., 179, 77-106, 2018.

Sipilä, M., Berndt, T., Petäjä, T., Brus, D., Vanhanen, J., Stratmann, F., Patokoski, J., Mauldin III, R. L., Hyvärinen, A.-P., and Lihavainen, H.: The role of sulfuric acid in atmospheric nucleation, Science, 327, 1243-1246, 2010.

Stone, D., Whalley, L. K., and Heard, D. E.: Tropospheric OH and HO 2 radicals: field measurements and model comparisons, Chemical Society Reviews, 41, 6348-6404, 2012.

https://doi.org/10.5194/egusphere-2025-861
Preprint. Discussion started: 26 June 2025

Takegawa, N., Seto, T., Moteki, N., Koike, M., Oshima, N., Adachi, K., Kita, K., Takami, A., and Kondo, Y.: Enhanced new particle formation above the marine boundary layer over the Yellow Sea: Potential impacts on cloud condensation nuclei, Journal of Geophysical Research: Atmospheres, 125, e2019JD031448, 2020.

Tham, Y. J., Sarnela, N., Iyer, S., Li, Q., Angot, H., Quéléver, L. L., Beck, I., Laurila, T., Beck, L. J., and Boyer, M.: Widespread detection of chlorine oxyacids in the Arctic atmosphere, Nature Communications, 14, 1769, 2023.

Thompson, C., Shepson, P., Liao, J., Huey, L., Apel, E., Cantrell, C., Flocke, F., Orlando, J., Fried, A., and Hall, S.: Interactions of bromine, chlorine, and iodine photochemistry during ozone depletions in Barrow, Alaska, Atmospheric Chemistry and Physics, 15, 9651-9679, 2015.

van Pinxteren, M., Fomba, K. W., van Pinxteren, D., Triesch, N., Hoffmann, E. H., Cree, C. H., Fitzsimons, M. F., von Tümpling, W., and Herrmann, H.: Aliphatic amines at the Cape Verde Atmospheric Observatory: Abundance, origins and sea-air fluxes, Atmos. Environ., 203, 183-195, 2019.

Williamson, C. J., Kupc, A., Axisa, D., Bilsback, K. R., Bui, T., Campuzano-Jost, P., Dollner, M., Froyd, K. D., Hodshire, A. L., and Jimenez, J. L.: A large source of cloud condensation nuclei from new particle formation in the tropics, Nature, 574, 399-403, 2019.

Wood, R.: Stratocumulus clouds, Monthly weather review, 140, 2373-2423, 2012.

Xie, H.-B., Elm, J., Halonen, R., Myllys, N., Kurten, T., Kulmala, M., and Vehkamaki, H.: Atmospheric fate of monoethanolamine: enhancing new particle formation of sulfuric acid as an important removal process, Environmental science & technology, 51, 8422-8431, 2017.

Yao, L., Garmash, O., Bianchi, F., Zheng, J., Yan, C., Kontkanen, J., Junninen, H., Mazon, S. B., Ehn, M., and Paasonen, P.: Atmospheric new particle formation from sulfuric acid and amines in a Chinese megacity, Science, 361, 278-281, 2018.

Yin, R., Yan, C., Cai, R., Li, X., Shen, J., Lu, Y., Schobesberger, S., Fu, Y., Deng, C., and Wang, L.: Acid–base clusters during atmospheric new particle formation in urban Beijing, Environmental Science & Technology, 55, 10994-11005, 2021.

Yu, H., Ren, L., Huang, X., Xie, M., He, J., and Xiao, H.: Iodine speciation and size distribution in ambient aerosols at a coastal new particle formation hotspot in China, Atmospheric Chemistry and Physics, 19, 4025-4039, 2019.

Zhang, R., Khalizov, A., Wang, L., Hu, M., and Xu, W.: Nucleation and growth of nanoparticles in the atmosphere, Chemical reviews, 112, 1957-2011, 2012.

Zhang, R., Suh, I., Zhao, J., Zhang, D., Fortner, E. C., Tie, X., Molina, L. T., and Molina, M. J.: Atmospheric new particle formation enhanced by organic acids, Science, 304, 1487-1490, 2004.

Zheng, G., Wang, Y., Wood, R., Jensen, M. P., Kuang, C., McCoy, I. L., Matthews, A., Mei, F., Tomlinson, J. M., and Shilling, J. E.: New particle formation in the remote marine boundary layer, Nature communications, 12, 527, 2021.

Zhu, Y., Li, K., Shen, Y., Gao, Y., Liu, X., Yu, Y., Gao, H., and Yao, X.: New particle formation in the marine atmosphere during seven cruise campaigns, Atmospheric Chemistry and Physics, 19, 89-113, 2019.

https://doi.org/10.5194/egusphere-2025-861
Preprint. Discussion started: 26 June 2025

Graphical Abstract

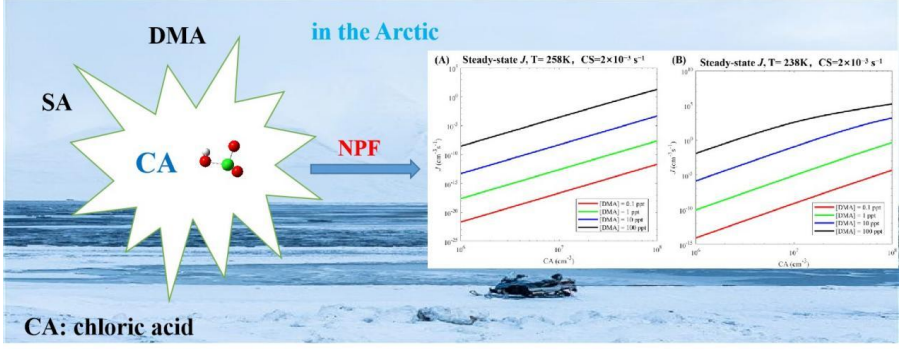

https://doi.org/10.5194/egusphere-2025-861
Preprint. Discussion started: 26 June 2025

Figure Captions

Figure 1. Identified lowest free energy structures of the $(CA)_{1-4}(DMA)_{1-4}$ clusters at the DLPNO-CCSD(T)/aug-cc-pVTZ//ωB97X-D/6-31++G(d,p) level of theory. The red, blue, gray, green and white balls represent oxygen, nitrogen, carbon, chlorine and hydrogen atoms, respectively. The dashed white and black lines indicate hydrogen and halogen bonds, respectively.

Figure 2. The formation free energy (ΔG) (in kcal mol^{-1}) of (A) $(CA)_{1-4}(DMA)_{1-4}$ and (B) $(CA)_{1-4}(SA)_{1-4}$ clusters at the DLPNO-CCSD(T)/aug-cc-pVTZ//ωB97X-D/6-31++G(d,p) level of theory. The calculations are performed at 278 K and 1 atm.

Figure 3. Evaporation rates for (A) $(CA)_{1-4}(DMA)_{1-4}$ and (B) $(CA)_{1-4}(SA)_{1-4}$ clusters

https://doi.org/10.5194/egusphere-2025-861
Preprint. Discussion started: 26 June 2025

clusters at 278 K and 1 am.

Figure 4. Simulated steady-state CA dimer concentration $\sum[(CA)_2]$ (cm^{-3}) (A) and the cluster formation rates J (cm^{-3} s^{-1}) out of the simulation systems (B) as a function of [CA] at 278 K.

Figure 5. The simulated cluster formation rate J (cm^{-3} s^{-1}) of the CA-DMA system at different temperatures (A) 258, and (B) 238 K; [CA] = 10^6 −10^8 molec. cm^{-3}; [DMA] = 0.1, 1, 10, and 100 ppt; and CS = 2×10^{-3} s^{-1}.

Figure 6. (A) Main clustering pathways of $(CA)_{1-4}(DMA)_{1-4}$ clusters at 278 K, [CA] = 10^6 cm^{-3}, and [DMA] = 1 ppt. (B) Main clustering pathways of $(CA)_{1-4}(SA)_{1-4}$ clusters at 278 K, [CA] = 10^6 cm^{-3}, and [SA] = 10^6 cm^{-3}.

https://doi.org/10.5194/egusphere-2025-861
Preprint. Discussion started: 26 June 2025

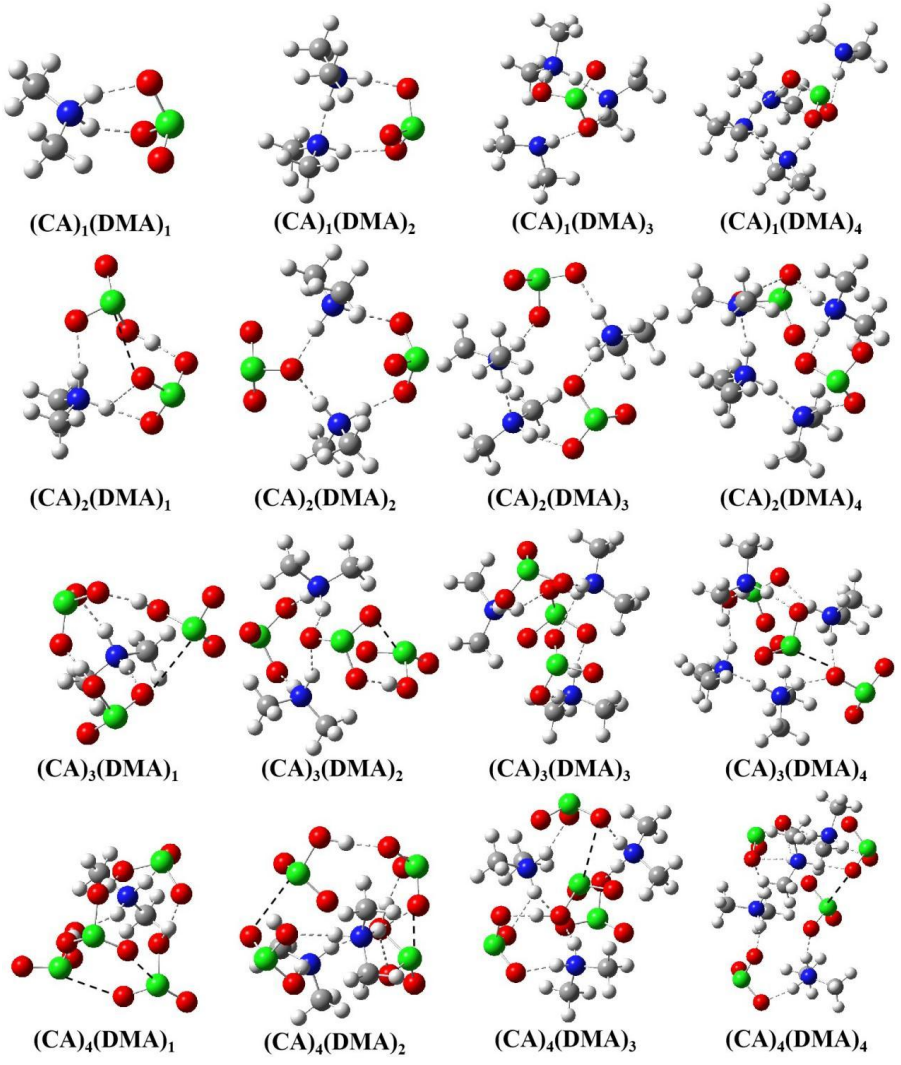

488

489 **Figure 1.** Identified lowest free energy structures of the $(CA)_{1-4}(DMA)_{1-4}$ clusters at
490 the DLPNO-CCSD(T)/aug-cc-pVTZ//ωB97X-D/6-31++G(d,p) level of theory. The
491 red, blue, gray, green and white balls represent oxygen, nitrogen, carbon, chlorine and
492 hydrogen atoms, respectively. The dashed white and black lines indicate hydrogen
493 and halogen bonds, respectively.

494

https://doi.org/10.5194/egusphere-2025-861
Preprint. Discussion started: 26 June 2025

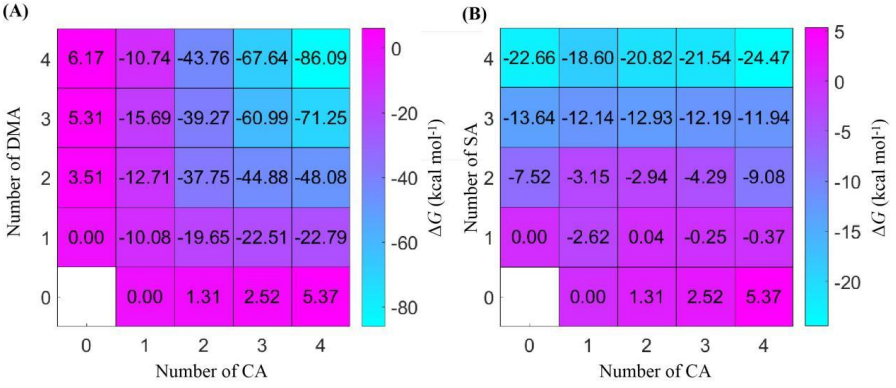

Figure 2. The formation free energy (ΔG) (in kcal mol^{-1}) of (A) $(CA)_{1-4}(DMA)_{1-4}$ and (B) $(CA)_{1-4}(SA)_{1-4}$ clusters at the DLPNO-CCSD(T)/aug-cc-pVTZ//ωB97X-D/6-31++G(d,p) level of theory. The calculations are performed at 278 K and 1 atm.

https://doi.org/10.5194/egusphere-2025-861
Preprint. Discussion started: 26 June 2025

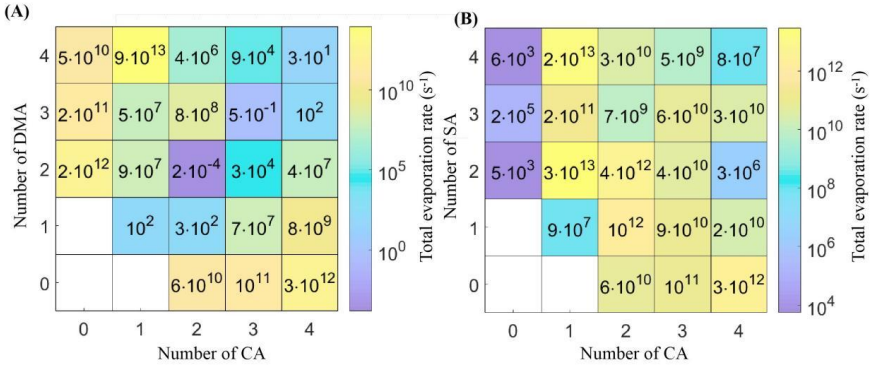

Figure 3. Evaporation rates for (A) $(CA)_{1-4}(DMA)_{1-4}$ and (B) $(CA)_{1-4}(SA)_{1-4}$ clusters clusters at 278 K and 1 am.

https://doi.org/10.5194/egusphere-2025-861
Preprint. Discussion started: 26 June 2025

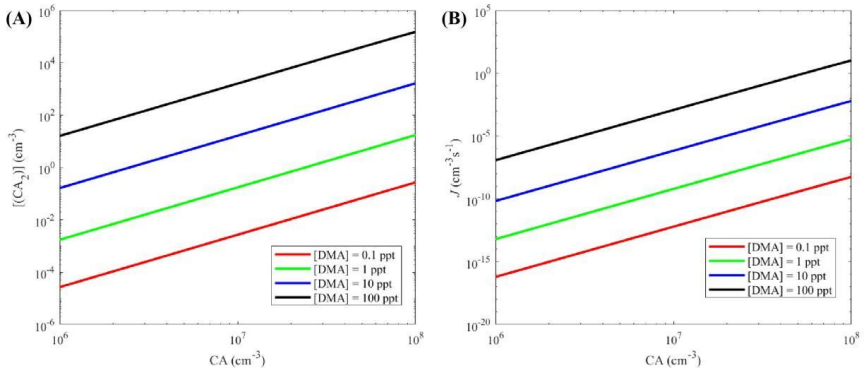

Figure 4. Simulated steady-state CA dimer concentration $\sum[(CA)_2]$ (cm^{-3}) (A) and the cluster formation rates J (cm^{-3} s^{-1}) out of the simulation systems (B) as a function of [CA] at 278 K.

https://doi.org/10.5194/egusphere-2025-861
Preprint. Discussion started: 26 June 2025

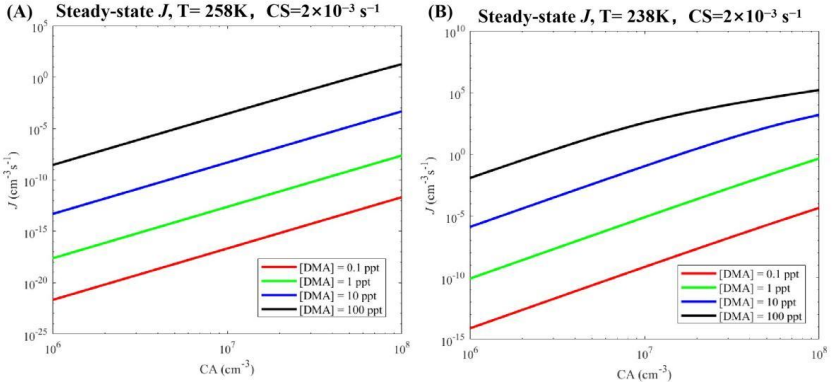

Figure 5. The simulated cluster formation rate J (cm^{-3} s^{-1}) of the CA-DMA system at different temperatures (A) 258, and (B) 238 K; [CA] = 10^6 −10^8 molec. cm^{-3}; [DMA] = 0.1, 1, 10, and 100 ppt; and CS = 2×10^{-3} s^{-1}.

https://doi.org/10.5194/egusphere-2025-861
Preprint. Discussion started: 26 June 2025

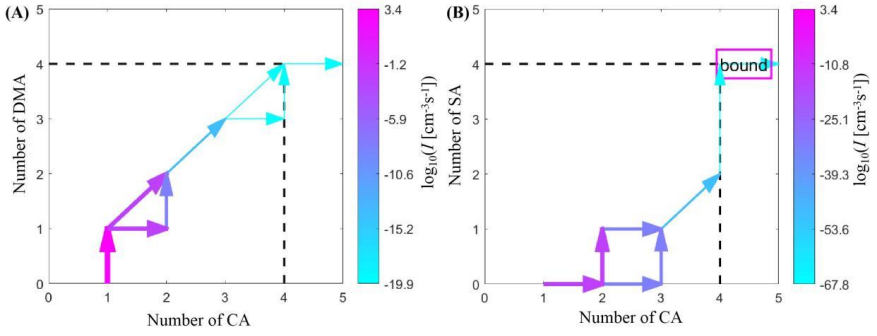

Figure 6. (A) Main clustering pathways of $(CA)_{1–4}(DMA)_{1–4}$ clusters at 278 K, [CA] = 10^6 cm^{-3}, and [DMA] = 1 ppt. (B) Main clustering pathways of $(CA)_{1–4}(SA)_{1–4}$ clusters at 278 K, [CA] = 10^6 cm^{-3}, and [SA] = 10^6 cm^{-3}.